Polyoxometalate HIV-1 Protease Inhibitors. A New Mode of Protease Inhibition

Deborah A. Judd,[†] James H. Nettles,[†] Neysa Nevins,[†] James P. Snyder,[†] Dennis C. Liotta,[†] Jordan Tang,[§] Jacques Ermolieff,[§] Raymond F. Schinazi,[‡] and Craig L. Hill*[,†]

Contribution from the Department of Chemistry, Emory University, Atlanta, Georgia 30322, Veterans Affairs Medical Center and Laboratory of Biochemical Pharmacology, Department of Pediatrics, Emory University School of Medicine, Decatur, Georgia 30033, and the Protein Studies Program, Oklahoma Medical Research Foundation and Department of Biochemistry and Molecular Biology, University of Oklahoma Health Sciences Center, Oklahoma City, Oklahoma 73104

Received May 24, 2000

Abstract: Nb-containing polyoxometalates (POMs) of the Wells−Dawson class inhibit HIV-1 protease (HIV-1P) by a new mode based on kinetics, binding, and molecular modeling studies. Reaction of α_1-$K_9Li[P_2W_{17}O_{61}]$ or α_2-$K_{10}[P_2W_{17}O_{61}]$ with aqueous H_2O_2 solutions of $K_7H[Nb_6O_{19}]$ followed by treatment with HCl and KCl and then crystallization affords the complexes α_1-$K_7[P_2W_{17}(NbO_2)O_{61}]$ (α_1**1**) and α_2-$K_7[P_2W_{17}(NbO_2)O_{61}]$ (α_2**1**) in 63 and 86% isolated yields, respectively. Thermolysis of the crude peroxoniobium compounds (72−96 h in refluxing H_2O) prior to treatment with KCl converts the peroxoniobium compounds to the corresponding polyoxometalates (POMs), α_1-$K_7[P_2W_{17}NbO_{62}]$ (α_1**2**) and α_2-$K_7[P_2W_{17}NbO_{62}]$ (α_2**2**), in moderate yields (66 and 52%, respectively). The identity and high purity of all four compounds were confirmed by ^{31}P NMR and ^{183}W NMR. The acid-induced dimerization of the oxo complexes differentiates sterically between the cap (α_2) site and the belt (α_1) site in the Wells−Dawson structure (α_2**2** dimerizes in high yield; α_1**2** does not). All four POMs exhibit high activity in cell culture against HIV-1 (EC_{50} values of 0.17−0.83 μM), are minimally toxic (IC_{50} values of 50 to >100 μM), and selectively inhibit purified HIV-1 protease (HIV-1P) (IC_{50} values for α_1**1**, α_2**1**, α_1**2**, and α_2**2** of 2.0, 1.2, 1.5, and 1.8 μM, respectively). Thus, theoretical, binding, and kinetics studies of the POM/HIV-1P interaction(s) were conducted. Parameters for $[P_2W_{17}NbO_{62}]^{7-}$ were determined for the Kollman all-atom (KAA) force field in Sybyl 6.2. Charges for the POM were obtained from natural population analysis (NPA) at the HF/LANL2DZ level of theory. AutoDock 2.2 was used to explore possible binding locations for the POM with HIV-1P. These computational studies strongly suggest that the POMs function not by binding to the active site of HIV-1P, the mode of inhibition of all other HIV-1P protease inhibitors, but by binding to a cationic pocket on the "hinge" region of the flaps covering the active site (2 POMs and cationic pockets per active homodimer of HIV-1P). The kinetics and binding studies, conducted after the molecular modeling, are both in remarkable agreement with the modeling results: 2 POMs bind per HIV-1P homodimer with high affinities ($K_i = 1.1 \pm 0.5$ and 4.1 ± 1.8 nM in 0.1 and 1.0 M NaCl, respectively) and inhibition is noncompetitive (k_{cat} but not K_m is affected by the POM concentration).

Introduction

This paper addresses the synthesis and characterization of polyoxometalates (POMs) that are active against HIV-1 and selectively inhibit HIV protease (HIV-1P) by a new mechanism based on multiple lines of experimental and corroborating theoretical evidence. Appropriately, brief backgrounds on the component disciplines follow: HIV chemotherapy and HIV-1P inhibitors, POMs and their antiviral chemistry, and modeling of POM−biomacromolecule interactions. HIV-1 (human immunodeficiency virus type 1) is the pathogen responsible for AIDS (acquired immunodeficiency syndrome). An essential step in the replication of HIV-1 is the proteolytic maturation of core proteins and enzymes encoded by the *gag* and *pol* genes.[1−5] The enzyme responsible for this function is HIV-1 protease (HIV-1P), an aspartyl protease similar to pepsin.[6,7] Disruption of this function produces morphologically immature and noninfectious virus particles.[8,9] HIV-1P inhibitors (PI) have received

[†] Department of Chemistry, Emory University.

[‡] Veterans Affairs Medical Center, the Georgia VA Research Center for AIDS and HIV Infections and Department of Pediatrics, Emory University School of Medicine.

[§] Oklahoma Medical Research Foundation.

(1) Debouck, C.; Gorniak, J. G.; Strickler, J. E.; Meek, T. D.; Metcalf, B. W.; Rosenberg, M. *Proc. Natl. Acad. Sci. U.S.A.* **1987**, *84*, 8903−8906.

(2) Abdel-Meguid, S.; Zhao, B.; Murthy, K. H. M.; Winborne, E.; Choi, J. K.; Desjarlais, R. L.; Minnich, M. D.; Culp, J. S.; Debouck, C.; Tomaszek, T. A., Jr.; Meek, T. D.; Dreyer, G. B. 1995, unpublished results.

(3) Meek, T. D.; Lamert, D. M.; Metcalf, B. W.; Petteway, S. R., Jr.; Dreyer, G. B. *Design of Anti-AIDS Drugs*; Elsevier: Amsterdam, 1990.

(4) Meek, T. D.; Lamert, D. M.; Dreyer, G. B.; Carr, T. S.; Tomaszek, T. A., Jr.; Moore, M. L.; Strickler, J. E.; Debouck, C.; Hyland, L. J.; Mathews, T. J.; Metcalf, B. W.; Petteway, S. R., Jr. *Nature* **1990**, *343*, 90−92.

(5) Abdel-Meguid, S. S.; Metcalf, B. W.; Carr, T. J.; Demarsh, P.; Des Jarlais, R. L.; Fisher, S.; Green, D. W.; Ivanoff, L.; Lambert, D. M.; Murthy, K. H. M.; Petteway, S. R., Jr.; Pitts, W. J.; Tomaszek, T. A., Jr.; Winborne, E.; Zhao, B.; Dreyer, G. B.; Meek, T. D. *Biochemistry* **1994**, *33*, 11671−11677.

(6) Meek, T. D.; Dayton, B. D.; Metcalf, B. W.; Dreyer, G. B.; Carr, T. S.; Strickler, J. E.; Gorniak, J. G.; Moore, M. L.; Rosenberg, M.; Magaard, V. W.; Debouck, C. *Proc. Natl. Acad. Sci. U.S.A.* **1989**, *86*, 1841−1845.

(7) Wlodawer, A.; Miller, M.; Jaskolski, M.; Sathanarayana, B. K.; Baldwin, E.; Weber, I. T.; Selk, L. M.; Clawson, L.; Schneider, J.; Kent, S. B. H. *Science* **1989**, *245*, 616−621.

(8) Jhoti, H.; Singh, O. M. P.; Weir, M. P.; Cooke, R.; Murrayrust, P.; Wonacott, A. *Biochemistry* **1994**, *33*, 8417−8427.

10.1021/ja001809e CCC: $20.00
Published on Web 01/12/2001

considerable attention as therapeutic agents against AIDS with peptide and peptidomimetics receiving the most attention.[10−13] Five derivatives (saquinavir, ritonavir, indinavir, nelfinavir, and amprenavir) were recently approved for use in humans by the Food and Drug Administration in conjunction with reverse transcriptase inhibitors, including nucleoside analogues.[14−16] However, several developments have hindered the development of these organic PIs. First, multistep syntheses are typically required resulting in an expensive product.[17,18] In addition, these drugs have poor pharmacokinetics, necessitating megadoses to achieve a sustained antiviral effect. Furthermore, they are metabolically unstable, have low oral bioavailability, and cannot be given with some other drugs because of drug interactions.[19,20] Last, there is increasing evidence that PIs induce lipodystrophy and hyperlipidemia.[21] In this investigation, we turned to early transition metal oxygen anion clusters (polyoxometalates or POMs for short) as potential protease inhibitors for two reasons. First, POMs are a large, diverse, and remarkably alterable class of inorganic compounds with recently reported biological data of significant promise (high efficacy and low toxicity; vide infra). Second, the sizes and globular structural motifs of many POMs are similar, and in some cases nearly identical to, the water-solubilized fullerene derivatives recently reported to have fairly good anti-HIV-1P activity.[22−25]

POMs are composed of d^0 cations (most commonly Mo^{VI}, W^{VI}, or V^{V}) bridged by oxide anions with structures comprised primarily of MO_6 units bridged by one, two, or in a few cases three oxygens.[26] These compounds are versatile because many of the properties that dictate their utility including elemental composition, structure, charge density, redox potential, acidity, and solubility can be controlled to varying degrees synthetically. POMs have been known for some time to have generically low cytotoxicity and broad spectrum antiviral activity.[22,25,27−48] More recently, the first rigorous pharmacokinetics studies on POMs were reported, and some compounds have been developed that are remarkably well tolerated in mammals.[29,48] Recent work also suggests that POMs have at least a dual mode of action: inhibition of HIV-1 reverse transcriptase (HIV-1 RT) inside cells and interference with viral entry and cellular fusion (inhibition of the binding of the HIV-1 surface protein, gp120, to the CD4 receptor protein on human lymphocytes).[25,39,49] Despite these promising events, the development of POMs as antiviral agents has been limited as many derivatives have little or no hydrolytic stability at physiologically relevant pH values (blood serum is typically pH 7.4).[42]

The new POMs of focus here are hydrolytically stable Nb-substituted heteropolytungstates of the Wells−Dawson class (polytungstodiphosphates). The two isomeric monosubstituted

(9) Kohl, N. E.; Emini, E. A.; Schleif, W. A.; Davies, L. J.; Heimbach, J. C.; Dixon, R. A. F.; Scholnick, E. M.; Sigal, I. S. *Proc. Natl. Acad. Sci. U.S.A.* **1988**, *85*, 4686−4690.
(10) Kim, E. E.; Baker, C. T.; Dwyer, M. D.; Murcko, M. A.; Rao, B. G.; Tung, R. D.; Navia, M. A. *J. Am. Chem. Soc.* **1995**, *117*, 1181−1182.
(11) Vara Prasad, J. V. N.; Para, K. S.; Lunney, E. A.; Ortwine, D. F.; Dunbar, J. B., Jr.; Ferguson, D.; Tummino, P. J.; Hupe, D.; Tait, B. D.; Domagala, J. M.; Humblet, C.; Bhat, T. N.; Liu, B.; Guerin, D. M. A.; Baldwin, E. T.; Erikson, J. W.; Sawyer, T. K. *J. Am. Chem. Soc.* **1994**, *116*, 6989−6990.
(12) Smith, A. B., III; Guzman, M. C.; Sprengeler, P. A.; Keenan, T. P.; Holcomb, R. C.; Wood, J. C.; Carroll, P. J.; Hirschmann, R. *J. Am. Chem. Soc.* **1994**, *116*, 9947−9962.
(13) Meek, T. D. *J. Enzymol. Inhib.* **1992**, *6*, 65−98.
(14) Moyle, G.; Gazzard, B. *Drugs* **1996**, *51*, 701−712.
(15) Deeks, S. G.; Smith, M.; Holodniy, M.; Kahn, J. O. *J. Am. Med. Assoc.* **1997**, *277*, 145−153.
(16) (a) Doran, C. M. *Ann. Pharmacother.* **1997**, *31*, 228−236. (b) Amprenavir approval: FDA paper, April 16, 1999, http://www.fda.gov.obs/topics/answers/ans00949.html. (c) Boden, D.; Markowitz, M. *Antimicrob. Agents Chemother.* **1998**, *42*, 2775−2783. (d) Molla, A.; Granneman, R.; Sun, E.; Kempf, D. *Antiviral Res.* **1998**, *39*, 1−23. (e) Jardine, D.; Tyssen, D.; Brich, C. *Antiviral Res.* **2000**, *45*, 59−68.
(17) Askin, D.; Eng, K. K.; Eossen, K.; Purick, R. M.; Wells, K. M.; Volante, R. P.; Reider, P. J. *Tetrahedron Lett.* **1994**, *34*, 673−676.
(18) Houpis, I. N.; Molina, A.; Reamer, R. A.; Lynch, J. E.; Volante, R. P.; Reider, R. A. *Tetrahedron Lett.* **1993**, *34*, 2593−2596.
(19) Plattner, J. J.; Norbeck, D. W. *Drug Discovery Technologies*; Ellis Horwood: Chichester, England, 1990.
(20) Kempf, D. J.; Codacoui, L.; Wang, X. C.; Kohlbrenner, W. E.; Wideburg, N. E.; Saldivar, A.; Vasavanonda, S.; Marsh, K. C.; Bryant, P.; Sham, H. L.; Green, B. E.; Betebenner, D. A.; Erickson, J. N.; Norbeck, D. W. *J. Med. Chem.* **1993**, *36*, 320−330.
(21) Carr, A.; Samaras, K.; Burton, S.; Law, M.; Freund, J.; Chisholm, D. J.; Cooper, D. A. *AIDS* **1998**, *12*, F51−F58.
(22) Schinazi, R. F.; Sijbesma, R.; Srdanov, G.; Hill, C. L.; Wudl, F. *Antimicrob. Agents Chemother.* **1993**, *37*, 1707−1710.
(23) Friedman, S. H.; DeCamp, D. L.; Sijbesma, R. P.; Srdanov, G.; Wudl, F.; Kenyon, G. L. *J. Am. Chem. Soc.* **1993**, *115*, 6506−6509.
(24) Sijbesma, R. P.; Srdanov, G.; Wudl, F.; Castoro, J. A.; Wilkins, C.; Friedman, S. H.; DeCamp, D. L.; Kenyon, G. L. *J. Am. Chem. Soc.* **1993**, *115*, 6510−6512.
(25) Rhule, J. T.; Hill, C. L.; Judd, D. A.; Schinazi, R. F. *Chem. Rev.* **1998**, *98*, 327−357.
(26) Recent reviews of POMs: (a) Pope, M. T.; Müller, A. *Angew. Chem., Int. Ed. Engl.* **1991**, *30*, 34−48. (b) *Polyoxometalates: From Platonic Solids to Anti-retroviral Activity*; Pope, M. T., Müller, A., Eds.; Kluwer Academic Publishers: Dordrecht, The Netherlands, 1993. (c) Hill, C. L. *Chem. Rev.* **1998**, *98*, 1 and 2 (special issue on polyoxometalates).
(27) Burgard, M.; Sansonetti, P.; Vittecoq, D.; Descamps, P.; Guetard, D.; Herson, S.; Rozenbaum, W.; Rouzioux, C. *AIDS* **1989**, *3*, 665−668.
(28) Moskovitz, B. L. *Antimicrob. Agents Chemother.* **1988**, *32*, 1300−1303.
(29) Ni, L.; Boudinot, F. D.; Boudinot, S. G.; Henson, G. W.; Bossard, G. E.; Martelucci, S. A.; Ash, P. W.; Fricker, S. P.; Darkes, M. C.; Theobald, B. R. C.; Hill, C. L.; Schinazi, R. F. *Antimicrob. Agents Chemother.* **1994**, *38*, 504−510.
(30) Yamamoto, N.; Schols, D.; De Clercq, E.; Debyser, Z.; Pauwels, R.; Balzarini, J.; Nakashima, H.; Baba, M.; Hosoya, M.; Snoeck, R.; Neyts, J.; Andrei, G.; Murrer, B. A.; Theobald, B.; Bossard, G.; Henson, G.; Abrams, M.; Picker, D. *Mol. Pharmacol.* **1993**, *42*, 1109−1117.
(31) Shigeta, S.; Mori, S.; Hosoya, M.; Baba, M.; Schinazi, R. F.; Hill, C. L. International Society for Antiviral Research, Charleston, SC, Feburary 27−March 4, 1994.
(32) Crans, D. C. *Comments Inorg. Chem.* **1994**, *16*, 35−76.
(33) Clayette, P.; Dormont, D. *Top. Mol. Org. Eng.* **1994**, *10*, 387−400.
(34) Inouye, Y.; Yoshida, T. *Nippon Rinsho (Jpn.)* **1993**, *51*, 186−191.
(35) Inouye, Y. *Kikan Kagaku Sosetsu* **1993**, *20*, 131−138.
(36) Inouye, Y.; Tokutake, Y.; Yoshida, T.; Yoshiko, S.; Hujita, H.; Dan, K.; Yamamoto, A.; Nishiya, S.; Yamase, T.; Nakamura, S. *Antiviral Res.* **1993**, *20*, 317−331.
(37) Baran, E. J. *Acta Farm. Bonaerense* **1993**, *11*, 155−160.
(38) Inouye, Y.; Tokutake, Y.; Kunihara, J.; Yoshida, T.; Yamase, T.; Nakata, A.; Nakamura, S. *Chem. Pharm. Bull.* **1992**, *40*, 805.
(39) Take, Y.; Tokutake, Y.; Inouye, Y.; Yoshida, T.; Yamamoto, A.; Yamase, T.; Nakamura, S. *Antiviral Res.* **1991**, *15*, 113−124.
(40) Schinazi, R. F.; Eriksson, B. F. H.; Chu, C. K.; Hill, C. L.; Arnold, B. H.; Cannon, D. L.; McClure, H.; Anderson, D.; Fultz, P. *Antiviral Res.* **1988**, *9*, 133.
(41) Hill, C.; Weeks, M.; Hartnup, M.; Sommadossi, J.-P.; Schinazi, R. *Ann. N.Y. Acad. Sci.* **1990**, *616*, 528−529.
(42) Hill, C.; Weeks, M.; Schinazi, R. F. *J. Med. Chem.* **1990**, *33*, 2767−2772.
(43) Hill, C. L.; Hartnup, M.; Faraj, M.; Weeks, M.; Prosser-McCartha, C. M.; Brown, R. B.; Schinazi, R. F.; Sommadossi, J.-P. *Polyoxometalates as Inorganic Anti-HIV-1 Compounds. Structure−Activity Relationships*; Diasio, R., Sommadossi, J.-P., Eds.; Pergamon: New York, 1990; pp 33−41.
(44) Hill, C.; Weeks, M.; Schinazi, R. F. *J. Med. Chem.* **1992**, *35*, 1216−1221.
(45) Kim, G.-S.; Judd, D. A.; Hill, C. L.; Schinazi, R. F. *J. Med. Chem.* **1994**, *37*, 816−820.
(46) Schinazi, R. F.; McMillan, A.; Juodawlkis, A. S.; Pharr, J.; Sijbesma, R.; Srdanov, G.; Hummelen, J.-C.; Boudinot, F. D.; Hill, C. L.; et al. *Proc. Electrochem. Soc.* **1994**, *94−24*, 689−96.
(47) Hill, C. L.; Kim, G.-S.; Prosser-McCartha, C. M.; Judd, D.; Pope, M. T., Müller, A., Eds.; Kluwer Academic Publishers: Dordrecht, Netherlands, 1993; pp 369−371.
(48) Blasecki, J. W. *Of Therapy, Toxicity and Tungstates: The Anti-Retroviral Pharmacology of Polyoxometalates*; Pope, M. T., Müller, A., Eds.; Kluwer Academic Publishers:The Netherlands, 1994; pp 373−385.
(49) Judd, D. A.; Schinazi, R. F.; Hill, C. L. *Antiviral Chem. Chemother.* **1994**, *5*, 410−14.

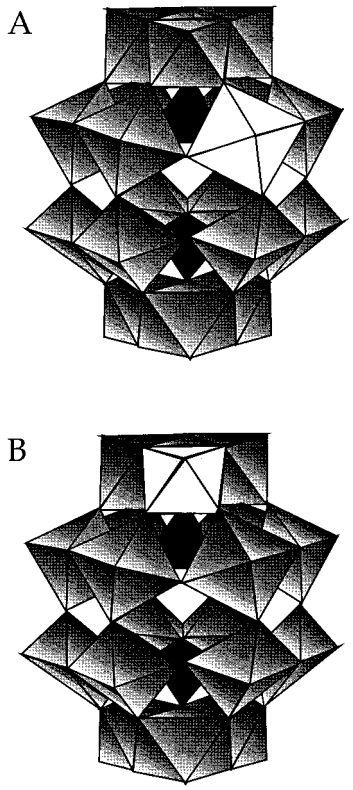

Figure 1. Polyhedral drawings of the two isomeric mononiobium-substituted polytungstodiphosphates. The lighter shaded polyhedra represent NbO_6 units and the dark internal tetrahedra represent PO_4 units: (A) the C_1 symmetry α_1 isomer, α_1-$[P_2W_{17}NbO_{62}]^{7-}$ (α_1**2**) and (B) the C_s symmetry α_2 isomer, α_2-$[P_2W_{17}NbO_{62}]^{7-}$ (α_2**2**). The peroxo derivatives are isostructural except that the terminal oxo groups on the Nb atoms are terminal peroxo groups.

peroxoniobium derivatives, α_1- and α_2-$K_7[P_2W_{17}(NbO_2)O_{61}]$ (α_1**1** and α_2**1**, respectively), as well as the corresponding oxoniobium derivatives, α_1- and α_2-$K_7[P_2W_{17}NbO_{62}]$ (α_1**2** and α_2**2**), have been synthesized, purified, and spectroscopically characterized.[50] These complexes, whose structures are illustrated in Figure 1, were targeted for three reasons: their structural motifs, their increased hydrolytic stability in basic media by substitution of Nb for W,[45,51−55] and their rational preparations (the defect precursors of α_1**1**, α_2**1**, α_2**2**, and α_1**2**, α_1- and α_2-$[P_2W_{17}O_{61}]^{10-}$, were obtained isomerically pure by Finke's group).[56]

These POMs, α_1**1**, α_2**1**, α_2**2**, and α_1**2**, exhibit concentrations for 50% inhibition (IC_{50} values) of HIV-1P in the 1−2 μM range and have no effect at 100 μM when evaluated against pepsin, a related aspartyl protease. The origins of this potent and selective inhibition have led us to investigate the potential molecular interactions between the POM α_2**2** and HIV-1P by computational methods and by experimental ones (kinetics and binding). Theoretical studies of molecules with MO_6 structural units are limited but growing. In 1992, Kempf and co-workers undertook an ab initio study of $[V_{10}O_{28}]^{6-}$ to investigate its electrostatic potential and gain insight into the relative basicities of the oxygens.[57] Recently, ab initio studies have been undertaken to determine, in part, structural properties and charges of oxovanadium alkoxides[58] and tungsten peroxocomplexes.[59] Molecular mechanics (MM) studies have also been reported recently. Cundari and co-workers used an MM approach to examine vanadium peroxides, deriving parameters from quantum mechanical calculations and approximations based on organic molecules with similar geometries.[60] Sarafianos, Pope, and co-workers evaluated a POM interacting with HIV-1 RT using SYBYL 6.1.[61] After charges were manually placed on the POM terminal oxygens, the POM/enzyme system was then optimized with the SYBYL force field and energies were reported. This study was the first to employ an MM-based method to gain insight into how POMs may inhibit enzyme function. In unpublished work, Crans and co-workers are exploring the docking of decavanadate with hexokinase.[62] POMs have not been well parametrized within a force field, and no systematic method has been developed to explore how they might interact with an enzyme. These problems, which were not considered by the original designers of force fields, are addressed here.

Experimental Section

Chemical Reagents and Methods. All chemicals and organic solvents were commercially available, reagent grade and used without further purification with the exception of Celite 545. Before use, the Celite was washed with a 4 M HCl solution and then rinsed with distilled water. Aqueous reactions were carried out in deionized water. The pH was measured using an Orion model 250A pH meter. The POMs $K_7H[Nb_6O_{19}]$,[52] α_2-$K_{10}[P_2W_{17}O_{61}]$,[63] α_1-$K_9Li[P_2W_{17}O_{61}]$,[63] $[NaP_5W_{30}O_{110}]^{14-}$,[64] and $[W_5NbO_{19}]^{3-}$ [51] were prepared by literature procedures. The purity and identification of the compounds were accessed by IR, ^{31}P NMR, ^{183}W NMR, and elemental analyses. IR spectra were obtained as KBr pellets (1−4 wt % in KBr) using a Nicolet 510M FTIR spectrometer. Elemental analyses were conducted by E + R Microanalytical Lab Inc. (Corona, NY). The ^{31}P and ^{183}W NMR spectra were run on a IBM WP-200SY FT spectrometer at 81.02 and 8.34 MHz, respectively. The ^{183}W NMR spectra of the peroxoniobium complexes were run on a Bruker 500 MHz instrument at the University of South Carolina. The probe temperature was 295 K in all NMR experiments. In reporting NMR data, chemical shifts upfield from the references are reported as negative values. The number of nuclei producing the resonance and line widths are reported. For ^{31}P NMR,

(50) Since our paper was first submitted and reviewed, Qu and co-workers have reported the preparation and characterization of some oxoNb Wells−Dawson POMs: cf. Gong, J.; Chen, Y.; Qu, L.; Qin. L. *Polyhedron* **1996**, *15*, 2273−2277.

(51) Dabbabi, M.; Boyer, M. *J. Inorg. Nucl. Chem.* **1976**, *38*, 1011−1014.

(52) Edlund, D. J.; Saxton, R. J.; Lyon, D. K.; Finke, R. G. *Organometallics* **1988**, *7*, 1692−1704.

(53) Pohl, M.; Lin, Y.; Weakley, T. J. R.; Nomiya, K.; Kaneko, M.; Weiner, H.; Finke, R. G. *Inorg. Chem.* **1995**, *34*, 767−777.

(54) Pohl, M.; Lyon, D. K.; Mizuno, N.; Nomiya, K.; Finke, R. G. *Inorg. Chem.* **1995**, *34*, 1413−1429.

(55) Day, V. W.; Klemperer, W. G.; Schwartz, C. *J. Am. Chem. Soc.* **1987**, *109*, 6030−6044.

(56) Lyon, D. K.; Miller, W. K.; Novet, T.; Domaille, P. J.; Evitt, E.; Johnson, D. C.; Finke, R. G. *J. Am. Chem. Soc.* **1991**, *113*, 7209−7221.

(57) Kempf, J. Y.; Rohmer, M. M.; Poblet, J. M.; Bo, C.; Benard, M. *J. Am. Chem. Soc.* **1992**, *114*, 1136−1146.

(58) Kempf, J. Y.; Maigret, B.; Crans, D. C. *Inorg. Chem.* **1996**, *35*, 6485−6494.

(59) Fantucci, P.; Lolli, S.; Venturello, C. *J. Catal.* **1997**, *169*, 228−239.

(60) Cundari, T. R.; Sisterhen, L. L.; Stylianopoulos, C. *Inorg. Chem.* **1997**, *36*, 4029−4034.

(61) Sarafianos, S. G.; Kortz, U.; Pope, M. T.; Modak, M. J. *Biochem. J.* **1996**, *319*, 619−626.

(62) Crans and co-workers have computationally investigated the binding of decavanadate to the minimally charged protein hexokinase. They have also experimentally investigated the binding of Keggin polytungstates with increasing numbers of substituted vanadium(V) centers (and consequent increasing molecular charge) to this protein. They find that POM−protein binding affinities (association constants) in this case involve more than simply molecular charge: Crans, D. C. and co-workers, presentation at Polyoxometalates: From Topology to Industrial Application, Center for Interdisciplinary Research, Bielefeld, Germany, October 2−6, 1999.

(63) Contant, R. *Inorg. Synth.* **1990**, *27*, 104−111.

(64) Alizadeh, M. H.; Harmalker, S. P.; Jeannin, Y.; Martin-Frère, J.; Pope, M. T. *J. Am. Chem. Soc.* **1985**, *107*, 2662−2669.

the samples were approximately 20 to 40 mM in POM and referenced to 85% H_3PO_4/D_2O. The spectra were run in Wilmad 513-7PP 10-mm i.d. NMR tubes. The pulse width was 14.8 μs, the relaxation delay was 1 s, and the acquisition time was 0.5 s. The concentration of POM was approximately 190 to 350 mM and the spectra were referenced to 2 M Na_2WO_4 in D_2O. The pulse width was 79.0 μs, the relaxation delay was 1 s, and the acquisition time was 4.096 s. For the ^{183}W NMR spectra of the peroxoniobium complexes, the concentration was approximately 350 mM, the pulse width was 24.0 μs, the relaxation delay was 5 ms, and the acquisition time was 2.261 s.

The number of peroxoniobium groups in these compounds was quantified by iodometric titration, using the procedure of Day and Underwood for H_2O_2.[65] The sodium thiosulfate titrant was standardized against potassium iodate with starch as the indicator.

Synthesis of α_1-$K_7[P_2W_{17}(NbO_2)O_{61}]\cdot 0.04KCl\cdot 13H_2O$ ($\alpha_1$1). Hexaniobate (0.66 g, 0.58 mmol $K_7H[Nb_6O_{19}]$) was dissolved in 100 mL of 0.5 M aqueous H_2O_2 (5 mL of a 30−35% aqueous solution dissolved in 95 mL of deionized water). HCl (3 mL of a 4 M aqueous solution) was added. The pH of the solution was approximately 1.5. A solution of α_1-$K_9Li[P_2W_{17}O_{61}]$ (7.9 g, 1.7 mmol) in 200 mL of a 0.5 M aqueous H_2O_2 solution with 1.0 M LiCl (10 mL of a 30−35% aqueous solution and 8 g of LiCl dissolved in 190 mL of deionized water) was added to the hexaniobate solution. To this was added approximately 10 mL of a 4 M aqueous HCl solution resulting in a final pH of 0.68. Potassium chloride (25 g, 0.31 mol) was added as a solid. The solution was concentrated down by blowing air over it for 24 h. A yellow amorphous solid mixed with a small amount of an orange crystalline solid was obtained. The reaction mixture was filtered and the filtrate maintained at 3 °C overnight to afford an orange crystalline solid (6.30 g, 1.38 × 10^{-3} mol, 63% yield). IR (1200−400 cm^{-1}): 1086, 1016, 957, 909, 776, 684, 595, 575, 561, 524. ^{31}P NMR (ppm; in H_2O with a D_2O coaxial tube): −11.0, −12.5. ^{183}W NMR (in H_2O with a D_2O coaxial tube; chemical shift, ppm ($^2J_{wow}$, Hz; line width, Hz)): −123.4 (20.8; 4.8), −125.2 (19.4; 4.3), −127.9 (ND; 6.1), −128.7 (ND; 3.9), −131.2 (20.8; 4.8), −135.2 (ND; 3.9), −140.6 (ND; 3.9), −157.8 (18.8; 4.3), −166.0 (20.8; 3.7), −172.2 (ND; 6.1), −172.5 (20.3; 4.8), −176.2 (25.4; 6.1), −179.7 (23.5; 4.0), −180.5 (19.9; 5.6), −183.9 (23.0; 4.8), −187.4 (21.2; 5.6), −213.3 (17.6; 6.1) (ND = not determinable). The number of peroxide groups was determined to be 1.08 ± 0.08 by iodometric titration. Elemental analysis (observed/calculated): H 0.66/0.55, K 6.23/5.74, Li <0.03/0, Nb 2.06/1.94, O (by difference) 24.85/25.34, P 1.11/1.29, W 65.06/65.13.

Synthesis of α_2-$K_{6.7}H_{0.3}[P_2W_{17}(NbO_2)O_{61}]\cdot 0.01KCl\cdot 15H_2O$ ($\alpha_2$1). $K_7H[Nb_6O_{19}]$ (0.42 g, 0.36 mmol) was dissolved in 50 mL of 0.5 M H_2O_2 (2.5 mL of a 30−35% aqueous solution dissolved in 47.5 mL of deionized water). HCl (1.5 mL of a 4 M aqueous solution) was added. The pH of the solution was approximately 1.3. A slurry of α_2-K_{10}-$[P_2W_{17}O_{61}]$ (5 g, 1.1 mmol) in 150 mL of a 0.5 M aqueous H_2O_2 (7.5 mL of a 30−35% aqueous solution dissolved in 143 mL of deionized water) was added to the hexaniobate solution. To this was added approximately 10 mL of a 4 M aqueous HCl solution resulting in a final pH of approximately 1 (0.89 to 0.94 on three separate syntheses). Potassium chloride (7.5 g, 0.094 mol) was added as a solid. The solution was concentrated down by blowing air over it for 24 h and then subsequently kept at 3 °C overnight. A yellow crystalline solid was collected (2.5 g, 5.48 × 10^{-4} mol). The supernatant was concentrated further by blowing air over the solution for 24 h. Refrigeration at 3 °C overnight afforded the yellow crystalline material (1.3 g, 2.85 × 10^{-4} mol). The supernatant was concentrated again by blowing air over it for 24 h and subsequent refrigeration overnight (3 °C) produced additional yellow crystalline material (0.54 g, 1.18 × 10^{-4} mol). The total yield was 4.34 g (9.51 × 10^{-4} mol, 86% yield). IR (1200−400 cm^{-1}): 1089, 1017, 956, 912, 778, 597, 563, 526. ^{31}P NMR (ppm; in H_2O with a D_2O coaxial tube): −10.9, −12.8. ^{183}W NMR (in H_2O with a D_2O coaxial tube; chemical shift, ppm (number of equivalent W atoms; $^2J_{wow}$, Hz; line width, Hz)): −107.7 (2W; 21.7; 3.7), −128.6 (2W; 20.4; 4.1), −141.6 (1W; 19.9; 3.7), −172.2 (2W; 24.8; 4.6), −176.1 (2W; 27.9; 5.9), −178.7 (2W; 20.3; 4.6), −183.0 (2W; 19.5; 4.6), −184.19 (2W; 21.2; 4.6), −189.5 (2W; 19.5; 4.5). The number of peroxide groups was determined to be 0.94 ± 0.05 by iodometric titration. Elemental analysis (observed/calculated): H 0.72/0.63, Cl 0.016/0.01, K 5.28/5.51, Nb 1.66/1.93, O (by difference) 26.47/25.86, P 1.12/1.28, W 64.73/64.78.

Synthesis of α_1-$K_{6.9}Li_{0.1}[P_2W_{17}NbO_{62}]\cdot 15H_2O$,($\alpha_1$2). The procedure used to prepare the α_1**1** complex was followed except that before the product was isolated, the solution was refluxed for 96 h to decompose the peroxo groups. After refluxing, the solution was filtered through acid-washed Celite. The solution was concentrated down to 250 mL on a hot plate and filtered again through acid-washed Celite. Potassium chloride (50 g, 0.67 mol) was added as a solid. The solution was concentrated down by blowing a stream of air over the solution. A pale yellow solid resulted (0.86 g, 0.189 mmol). The solution was concentrated down further on a hot plate. The solution turned from pale yellow to bright yellow. The solution was cooled to room temperature and 6.70 g of a pale yellow solid mixed with a flaky white solid (KCl) precipitated out. This solid was dissolved in a minimum amount of hot water and a light green-yellow crystalline solid resulted (total yield 4 g, 8.8 × 10^{-4} mol, 66% yield). IR (1200−400 cm^{-1}): 1090, 1018, 959, 908, 778, 596, 562, 518. ^{31}P NMR (ppm; in H_2O with a D_2O coaxial tube): −10.7, −12.5. ^{183}W NMR (in H_2O with a D_2O coaxial tube; chemical shift, ppm (line width, Hz)): −121.3 (4.9), −123.6 (ND), −124.1 (ND), −130.8 (2.8), −135.7 (3.2), −149.0 (2.2), −151.8 (2.1), −156.3 (4.7), −168.0 (2.0), −172.2 (1.5), −175.7 (1.6), −179.6 (2.3), −181.3 (2.4), −184.2 (ND), −184.8 (ND), −187.5 (2.2), and −208.1 (6.5) (ND = not determinable). Elemental analysis (observed/calculated): H 0.66/0.63, K 6.23/5.61, Li <0.03/0.01, Nb 2.06/1.93, O (by difference) 24.85/25.60, P 1.11/1.29, W 65.06/64.94.

Synthesis of α_2-$K_7[P_2W_{17}NbO_{62}]\cdot 0.04KCl\cdot 13H_2O$ ($\alpha_2$2). The initial procedure for the synthesis of the peroxoniobium complex, α_2**1**, was followed. Before addition of KCl, however, the reaction mixture was heated under reflux for 72 h to decompose the peroxo groups. The solution was filtered through acid-washed Celite three times. The filtrate was concentrated on a hot plate to a volume of approximately 200 mL (the color of the solution changed from very pale yellow to bright yellow). After the solution was cooled to room temperature, KCl (12 g, 0.161 mol) was added. A very pale green-yellow solid resulted (5.65 g, 1.2 × 10^{-3} mol). The solid was recrystallized from hot water (5.22 g, 0.0011 mol, 52% yield). IR (1200−400 cm^{-1}): 1089, 1019, 956, 911, 770, 597, 564, 524, 485, 473. ^{31}P NMR (ppm; in H_2O with a D_2O coaxial tube): −10.7, −12.9; ^{183}W NMR (in H_2O with a D_2O coaxial tube; chemical shift, ppm (number of equivalent W atoms; $^2J_{wow}$, Hz; line width, Hz)): −109.5 (2W; 20.6; 2.3), −128.7 (2W; 19.9; 3.4), −153.4 (1W; 18.3; 2.3), −156.7 (2W; 24.4; 4.1), −176.5 (2W; 22.0; 2.5), −182.5 (2W; 14.0; 1.4), −185.0 (2W; ND; 2.0), −186.6 (2W; ND; 2.4), and −198.2 (2W; 20.6; 2.9) (ND = not determinable). Elemental analysis (observed/calculated): H 0.51/0.55, Cl <0.03/0.03, K 5.75/5.75, Nb 1.95/1.94, O (by difference) 24.83/25.09, P 1.30/1.30, W 65.63/65.34.

pH Stability. ^{31}P NMR spectra were conducted at various pH values. A coaxial tube containing 1% trimethyl phosphate (TMP) in D_2O was used as an external standard. Due to the long T_1 of TMP, a relaxation delay of 2.5 s was used to ensure that the TMP was fully relaxed before the next pulse. The samples were dissolved in D_2O. The pD was measured on a Corning model 240 pH meter. pH and pD are related by the following equation: pH = pD − 0.48.

HIV-1 Protease Investigations. (a) Materials. Recombinant HIV-1P was prepared from *Escherichia coli* inclusion bodies by refolding and purified according to previously published procedures.[66,67] Chromogenic substrate, Lys-Ala-Arg-Val-Leu-Nph-Glu-Ala-Met (Nph = *p*-nitrophenylalanine), was synthesized at the Molecular Biology Resource Center, University of Oklahoma Health Sciences Center, using an Applied Biosystems peptide synthesizer 430A.

(b) Determination of K_m and k_{cat} The kinetic constants for the hydrolysis of Lys-Ala-Arg-Val-Leu-Nph-Glu-Ala-Met by HIV-1P (0.15

(65) Day, R. A., Jr.; Underwood, A. L. *Quantitative Analysis*, 5th ed.; Prentice Hall: Englewood Cliffs, NJ, 1986.

(66) Ido, E.; Han, H.-P.; Kezdy, F. J.; Tang, J. *J. Biol. Chem.* **1991**, *266*, 24359−24366.

(67) Lin, Y.-Z.; Lin, X.; Hong, L.; Foundling, S.; Heinrikson, R. L.; Thaisrivongs, S.; Leelamanit, W.; Raterman, D.; Shah, M.; Dunn, B. M.; Tang, J. *Biochemistry* **1994**, *34*, 1143−1152.

μM) were determined with several concentrations of the POM α_2**2** by adding constant concentrations of enzyme to variable concentrations of substrate. The initial rates of substrate hydrolysis were monitored at 300 nm with a Varian DMS 300 spectrophotometer. The initial velocities were fitted to the Michealis-Menten equation using the Enzfitter program[68] to obtain k_{cat} and K_m values. All the experiments were performed in 0.1 M sodium acetate with 0.1 M NaCl and 1% dimethyl sulfoxide at pH 5 and 37 °C.

(c) Stoichiometry and Inhibition Constant, K_i. Binding stoichiometry and K_i values for the POM α_2**2** were measured by adding increasing amounts of this compound to a constant amount of HIV-1P (0.15 μM) and measuring the residual enzyme activities with the chromogenic substrate (0.15 mM). Two sets of experiments were carried out in the previous acetate buffer with 0.1 and 1.0 M NaCl. K_i was calculated with eq 1 for the hyperbolic tight binding inhibitors:[69]

$$\frac{v_i}{v_o} = \frac{v_o - v_\infty}{2v_o}\left(\sqrt{\left(A + \frac{[I]_o}{[E]_o} - 1\right)^2 + 4A} + \frac{v_o + v_\infty}{v_o - v_\infty} - A - \frac{[I]_o}{[E]_o}\right) \quad (1)$$

where

$$A = \frac{1 + [S]_o/K_m}{\alpha + [S]_o/K_m}\frac{\alpha K_i}{[E]_o}$$

$[I]_o$ = [POM]/number of binding sites; $\alpha = K_m$ in the presence of a saturating concentration of POM/K_m in the absence of POM; v_i/v_o = the rate of substrate hydrolysis in the presence of POM/rate of substrate hydrolysis in the absence of POM; v_∞ is the limit of v_i for a saturating concentration of POM. Equation 1 takes into account both the tight-binding behavior of POM and the residual enzymatic activity of the HIV-1P−POM complex. To calculate α, we measured separately K_m in the absence and presence of POM. In our case the value of K_m is not affected by POM and therefore $\alpha = 1$.

(d) POM Inhibitory Concentrations. The inhibition of HIV-1P activity was analyzed using a chromogenic substrate: Lys-Ala-Arg-Val-Leu-Nph-Glu-Ala-Met (Nph is *p*-nitrophenylalanine). The assay was carried out at 37 °C in 0.1 M sodium acetate, pH 5.0, containing 0.1 M NaCl with HIV-1P and substrate concentrations of 0.41 μM and 0.22 μM, respectively. The hydrolysis rate was followed by the absorbance at 300 nm on a HP8452 diode array spectrophotometer equipped with a temperature control unit. The IC_{50} values were determined from the plot of inhibitor concentrations versus initial hydrolysis velocities. To determine the specificity of these compounds, pepsin, an aspartyl protease, was used for comparison.

The POMs were evaluated for anti-HIV-1 activity and toxicity in human mitogen-stimulated peripheral blood mononuclear cells (PBMC) infected with HIV-1 (LAI strain) as previously described.[45,70−72]

(e) General Theoretical Approach. A major goal of this study was to develop a reasonable method for studying the POM/HIV-1P system computationally. If an X-ray crystal structure is available for an enzyme, its interactions with a potential inhibitor can be assessed with a variety of molecular modeling tools. Visualization programs allow one to inspect and measure molecules and possibly aid the user in making qualitative estimates of potential interactions. Molecular mechanics provides a relatively quick and meaningful way to evaluate molecular structures and energies, provided that reasonable parameters are in place for the molecules of interest. In the present situation, since POMs are fairly rigid structures coated with oxygen atoms bearing partial negative charges that provide the sole interaction sites with the protein, we have chosen not to develop specific empirically based parameters for the POM internal metal atoms, heteroatoms or oxygen atoms. Instead, an alternative three-point strategy is adopted. First, the rigid X-ray crystal shape of the POM is faithfully maintained throughout all computational exercises. Second, the external oxygen atoms are provided with good charges fully consistent with the existence of internal metal cores in the actual POM. Third, following a determination of steric fit, electrostatic interactions are allowed to guide the details of mutual orientation of POM and enzyme. This straightforward scheme is remarkably successful in predicting the stoichiometry and kinetics of the POM−protein complex in the present case. It may well be sufficiently general to serve at least as a starting point for other POM−protein encounters.

With the above in mind, starting coordinates for the modeling studies were obtained from X-ray crystallographic data. All structures containing HIV-1P were obtained by anonymous FTP from the Brookhaven National Protein Data Bank.[73] To obtain measurements for the "closed" form of the HIV-1P active site, systems of HIV-1P bound to synthetic inhibitors were used.[74,75] A structure of HIV-1P in its unbound open form, solved by Wlodawer and co-workers, was used for active site measurement, exploration, and computation.[7] The structure for the "Wells Dawson" class POM was obtained from the Karlsruhe Inorganic Crystal Structure Database (ICSD).[76] All systems were graphically modeled in Sybyl 6.2[77] on Silicon Graphics Workstations. Enzyme calculations were performed by using the Kollman all-atom (KAA) force field[78] in Sybyl 6.2 on a Silicon Graphics Power Challenge. MOLCAD software was used for qualitative surface and electrostatic visualization of HIV-1P and the POM.[79−81] POM molecular orbital calculations were carried out using Gaussian94[82] on an IBM SP2 at the Cherry L. Emerson Center for Scientific Computation. Details of the structural modifications and computational methods are explained below.

(f) Measurements of Steric Environments of POM and HIV-1P. Structurally, HIV-1P has been extensively characterized while complexed with small synthetic organic or peptidic inhibitors and to a lessor extent in an unbound form. Structures of HIV-1P complexed with peptidomimetic inhibitors have structural and electrostatic similarities,

(68) Leatherbarrow, R. J. *ENZFITTER. A Nonlinear Regression Data Analysis Program for the IBMC PC*; Elsevier Science Publishers: Amsterdam, The Netherlands, 1987.

(69) Szedlacsek, S. E.; Ostafe, V.; Serban, M.; Vlad, M. O. *Biochem. J.* **1988**, *254*, 311−312.

(70) Schinazi, R. F.; Sommadossi, J.-P.; Saalmann, V.; Cannon, D. L.; Xie, M. W.; Hart, G. C.; Smith, G. A.; Hahn, E. F. *Antimicrob. Agents Chemother.* **1990**, *34*, 1061−1067.

(71) Bardos, T. J.; Schinazi, R. F.; Ling, K.-H. J.; Heider, A. R. *Antimicrob. Agents Chemother.* **1992**, *36*, 108−114.

(72) Chou, J.; Chou, T.-C.; Dose−effect analysis with microcomputers: Quantitation of ED_{50}, LD_{50}, synergism, antagonism, low-dose risk, receptor binding, and enzyme kinetics. *A computer software for Apple II Series and IBM-PC and Instruction Manual Elsevier-Biosoft*; Elsevier Science Publishers: Cambridge, UK, 1985.

(73) Abola, E. E.; Bernstein, F. C.; Bryant, S. H.; Koetzle, T. F.; Weng, J. *Protein Data Bank*; Allen, F. H., Bergerhoff, G., Sievers, R., Eds.; Data Commission of the International Union of Crystallography: Bonn/Cambridge/Chester, 1987; pp 107−132.

(74) Wlodawer, A.; Erickson, J. W. *Annu. Rev. Biochem.* **1993**, *62*, 543−585.

(75) Lam, P. Y. S.; Jadhav, P. K.; Eyermann, C. J.; Hodge, C. N.; Ru, Y.; Bacheler, L. T.; Meek, J. L.; Otto, M. J.; Rayner, M. M.; Wong, Y. N.; Chang, C. H.; Weber, P. C.; Jackson, D. A.; Sharpe, T. R.; Erickson-Viitanen, S. *Science* **1994**, *263*, 380−384.

(76) Finke, R. G.; Lyon, D. K.; Nomiya, K.; Weakley, T. J. R. *Acta Crystallogr.* **1990**, *C46*, 1592−1596.

(77) *Sybyl 6.2*; TRIPOS, Inc., 1699 S. Hanley Road, St. Louis, MI, 1991−1995.

(78) Weiner, S. J.; Kollman, P. A.; Nguyen, D. T.; Case, D. A. *J. Comput. Chem.* **1986**, *7*, 230−252.

(79) Connolly, M. L. *Science* **1983**, *221*, 709−713.

(80) Waldherr-Teschner, M.; Goetze, T.; Heiden, W.; Knoblauch, M.; Vollhardt, H.; Brickmann, J. *MOLCAD−Computer Aided Visualization and Manipulation of Models in Molecular Science*; Post, F. H., Hin, A. J. S., Eds.; Springer: Heidelberg, 1992; pp 58−67.

(81) Brickmann, J.; Goetze, T.; Heiden, W.; Moeckel, G.; Reiling, S.; Vollhardt, H.; Zachmann, C.-D. *Interactive Visualization of Molecular Scenarios with MOLCAD/SYBYL*; Bowie, J. D., Ed.; Addison-Wesley Publishing Co., Inc.: Reading, MA, 1995; pp 83−97.

(82) Frisch, M. J.; Trucks, G. W.; Schlegel, H. B.; Gill, P. M. W.; Johnson, B. G.; Robb, M. A.; Cheeseman, J. R.; Keith, T.; Petersson, G. A.; Montgomery, J. A.; Raghavachari, K.; Al-Laham, M. A.; Zakrzewski, V. G.; Ortiz, J. V.; Foresman, J. B.; Cioslowski, J.; Stefanov, B. B.; Nanayakkara, A.; Challacombe, M.; Peng, C. Y.; Ayala, P. Y.; Chen, W.; Wong, M. W.; Angres, J. L.; Replogle, R.; Gomperts, R.; Martin, R. L.; Fox, D. J.; Binkley, J. S.; Defrees, D. J.; Baker, J.; Stewart, J. P.; Head-Gordon, M.; Gonzales, C.; Pople, J. A. *Gaussian 94*, revision D.3; Pittsburgh, PA, 1995.

Table 1. Ab Initio Calculations on $WO_2(OH)_2$ with Natural Population Analysis (NPA) and Mulliken (MUL) Partial Charge Analysis

	HF/LANL2DZ		HF/6-31G		HF/6-31+G		HF/6-31G*	
	NPA	MUL	NPA	MUL	NPA	MUL	NPA	MUL
=O	−0.83	−0.62	−0.85	−0.71	−0.85	−0.65	−0.87	−0.73
W	2.76	2.25	2.82	2.70	2.82	2.30	2.85	2.46
O	−1.11	−0.99	−1.13	−1.23	−1.13	−0.99	−1.09	−1.02
H	0.56	0.49	0.58	0.59	0.58	0.49	0.54	0.51
	Becke3LYP/LANL2DZ		Becke3LYP/6-31G		Becke3LYP/6-31 + G		Becke3LYP/6-31G*	
	NPA	MUL	NPA	MUL	NPA	MUL	NPA	MUL
=O	−0.69	−0.45	−0.69	−0.48	−0.70	−0.60	−0.71	−0.53
W	2.24	1.56	2.23	1.60	2.29	2.23	2.29	1.72
O	−0.99	−0.76	−0.97	−0.76	−1.01	−1.05	−0.96	−0.79
H	0.55	0.43	0.54	0.44	0.56	0.53	0.53	0.46
	MP2/LANL2DZ		MP2/6-31G		MP2/6-31 + G		MP2/6-31G*	
	NPA	MUL	NPA	MUL	NPA	MUL	NPA	MUL
=O	−0.83	−0.63	−0.83	−0.66	−0.84	−0.70	−0.88	−0.76
W	2.77	2.26	2.76	2.30	2.81	2.60	2.88	2.74
O	−1.13	−1.01	−1.12	−0.99	−1.15	−1.19	−1.13	−1.21
H	0.58	0.50	0.58	0.50	0.59	0.59	0.56	0.60

especially the hydrogen-bonding patterns between the active site side chains and P3′−P3 inhibitor residues.[83] All known inhibitors are bound to HIV-1P in its closed form. The geometry of the POM-protein system was examined with respect to four structures of HIV-1P bound to an inhibitor. Measurements were made within Sybyl and numerical results are presented in the Results section. Since the POM is clearly unable to bind within the binding site of the closed form of HIV-1P, the open form was examined.

Although no structures of HIV-1P complexing in an open form are available, there is literature precedent for the possibility. In a study by Friedman and co-workers, fullerenes were proposed as candidate inhibitors of HIV-1P due to shape complimentarity.[23] The fullerenes were modeled in the open active site of the native enzyme structure of Wlodawer et al.[7] We have used this system as a model to examine the potential for a POM to bind in a similar way. The fullerene binding postulate was based on an estimate of displaced solvent volume and hydrophobic surface complimentarity. Due to the anionic character of the POM, we have treated the system using a molecular mechanics force field to evaluate the steric and electronic environment.

(g) Structural Parameters. Bond lengths and angles were derived from the X-ray structure of the Wells−Dawson complex $Na_9[P_2W_{15}Nb_3O_{62}]$ by Finke, Weakley, and co-workers.[76] This structure is a prolate ellipsoid (shaped like an American football; the general Wells−Dawson POM structure is illustrated in Figure 1). There are three tungstens in one cap, three niobiums in the other cap, and two belts of six tungstens each. An internal phosphate coordinates the cap and the belt regions. There are 18 terminal and 44 bridging (36 two-, 6 three-, and 2 four-coordinated) oxygens.

Since no X-ray crystal structure is available for the $[P_2W_{17}NbO_{62}]^{7-}$ anion, two of the three niobiums in the Nb_3 cap of $[P_2W_{15}Nb_3O_{62}]^{9-}$ were replaced by tungsten, and the sodium cations and cocrystallized solvent molecules were removed. Next, the $[P_2W_{17}NbO_{62}]^{7-}$ structure was defined as an aggregate within Sybyl. It was hoped that with simple addition of van der Waals parameters and partial charges, the POM could be studied in the context of HIV-1P. However, a variety of straightforward optimization schemes either failed to converge or led to unrealistic deformation of protein side-chains and loops. As a consequence, a number of dummy atoms and parameters were defined for POM atoms and employed in connection with various force field constraints. The details follow.

A script was written with the Sybyl programming language (SPL) to add constraints to the 116 bond lengths and 348 bond angles in the POM. An atom type scheme was defined for metals (W, Nb) and oxygens (Ot (terminal), Ob (bridging), O3 (three-coordinated), O4 (four-coordinated)). Constraint force parameters were assigned to be an order of magnitude larger than average parameters within the KAA force field, with values of 4000 kcal/[(mol)(Å)^2] and 4000 kcal/[(mol)(rad)^2] for the stretching and bending force parameters, respectively. All other force parameters within the KAA force field were assigned values of zero so that optimization proceeded without termination due to the lack of parameters. In other words, although the constraint values override the KAA parameters, if no default KAA parameters are in the force field, the calculation is interrupted with an error message. The experimental X-ray values were used for the natural bond lengths and angles. All torsional parameters were given values of zero, since the caged structure has low torsional flexibility.

(h) Determination of POM Charges. Partial charges for each atom of the POM were determined from natural population analysis[84] following restricted Hartree−Fock (RHF) calculations with the LANL2DZ basis set.[85−87] This basis set includes an effective core potential (ECP), which has been developed to treat transition metals.[85] Mulliken charges have been found to be more basis set dependent than NPA values, while the latter provide consistent charges for double-ζ and higher basis sets.[88] To assess the viability for determining partial charges for the atoms in the POM units, calculations were initially carried out on smaller systems. The neutral molecule $WO_2(OH)_2$ was optimized at various levels of theory, and Mulliken and NPA charges were determined (Table 1).

NPA charges for $WO_2(OH)_2$ are relatively constant for double-ζ type basis sets, regardless of the level of theory (RHF, Becke3LYP, or Møller−Plesset) or the addition of diffuse or polarization functions. The Mulliken charges, however, show considerable variation. To verify charge consistency for POM systems, a single-point RHF/LANL2DZ calculation (geometry from X-ray structure) was also undertaken for a smaller hexametalate $[W_6O_{19}]^{2-}$.[89] Charges for this system (tungstens, terminal and bridging oxygens) are shown in Table 2 and are consistent with those for **2** and $WO_2(OH)_2$.

Once the HF/LANL2DZ level of theory and the NPA method for deriving partial charges were selected, the question of how to treat the actual POM needed to be addressed. The entire $[P_2W_{17}NbO_{62}]^{7-}$ molecule is too large to calculate directly. Thus, it was divided into two halves, with the central bridging oxygens included in each half. Single-point RHF/LANL2DZ calculations were then carried out on each

(83) Gustchina, A.; Sansom, C.; Prevost, M.; Richelle, J.; Wodak, S. Y.; Wlodawer, A.; Weber, I. T. *Protein Eng.* **1994**, *7*, 309−317.
(84) Reed, A. E.; Weinstock, R. B.; Weinhold, F. *J. Chem. Phys.* **1985**, *83*, 735−746.
(85) Wadt, W. R.; Hay, P. J. *J. Chem. Phys.* **1985**, *82*, 270−283.
(86) Hay, P. J.; Wadt, W. R. *J. Chem. Phys.* **1985**, *82*, 299−310.
(87) Wadt, W. R.; Hay, P. J. *J. Chem. Phys.* **1985**, *82*, 284−298.
(88) Bachrach, S. M. *Population Analysis and Electron Densities from Quantum Mechanics*; VCH Publishers: New York, 1994; Vol. 5, pp 171−227.
(89) Fedin, V. P.; Mironov, Y. V.; Virovets, A. V.; Podberezskaya, N. V.; Federov, V. Y. *Polyhedron* **1992**, *11*, 1959−1963.

Table 2. Charges Determined from a HF/LANL2DZ Single-Point Calculation on $[W_6O_{19}]^{2-}$

	NPA	MUL
W	2.37	2.46
terminal O	−0.74	−0.63
bridging O	−1.05	−0.97
6-coordinated O	−1.38	−1.30

half. Naturally, the oxygen atoms intended to connect the two halves are terminal rather than bridging. This leads to calculated partial charges that are higher than those for the bridging oxygens completely internalized within each POM half. As a result, for the doubled, intact POM unit, the charges on the oxygen atoms linking the halves were reduced to values very close to those of the other bridging oxygen atoms. This expediency simultaneously delivered an overall charge on the POM in accord with its experimental value. The entire charge set was transferred to the KAA force field.

Hydrogen bonding terms for C═O···H−O and C═O···H−N were used in the force field for both terminal and bridging oxygens hydrogen bonded to hydroxyl and amine hydrogens. To determine hydrogen-bonding distances and angles, calculations on H_5WO_6 subsystems interacting with water and small amine-containing compounds were carried out at the RHF level of theory using the LANL2DZ basis set for W and the 6-31G* basis set for O and H. The standard KAA hydrogen bonding terms for C═O···H−O and C═O···H−N were implemented for both monovalent and divalent oxygens interacting with hydroxyl and amine hydrogens, respectively, and were adequate for reasonably reproducing the ab initio geometries.

This method of parametrization worked well, resulting in an optimized POM that deviated by less than 0.1 Å from the crystal structure.

(i) Surface Analysis. MOLCAD Connolly surfaces were generated within the SYBYL interface for the POM and HIV-1P structures with use of a 1.4 Å probe radius. Electrostatic potential color gradients were mapped to the surfaces by using NPA charges derived for the POM and KAA charges for the HIV-1P. The system was analyzed visually by using manual docking. The POM and the entire HIV-1P were examined for shape, size, and electrostatic complimentarity with each other. The observed qualitative results prompted us to quantitatively examine possible interactions.

(j) Docking Study of POM in HIV-1P. The structure used in this study was deposited in the Brookhaven National Protein Data Bank as a monomer, PDB ID code 3HVP. The mutant system required structural modification to resemble the wild-type by modification of the α-amino-*n*-butyric acid residues 67 and 95 to cysteines. The open form of the HIV-1P dimer was generated by using the crystallographic space group and unit cell parameters provided with the monomer coordinates. After KAA atom types were applied, the dimer was minimized with 500 steps of steepest descent, using a 16 Å nonbonded cutoff distance and a dielectric constant of 4.0.

The program AutoDock 2.2 was used to allow the POM to explore orientations in the active site of HIV-1P.[90] AMBER united-atom charges were placed on all heavy atoms and essential hydrogens of the enzyme in such a way as to produce a neutral POM-enzyme complex. A 12-6 Leonard-Jones potential accounts for van der Waals interactions (12-10 for hydrogen bonds). In this case, each atom type (effectively oxygen only) in the POM "probes" a grid (defined by the active site). Electrostatic energies are calculated at each grid point for each POM atom.

A Monte Carlo simulated annealing algorithm in conjunction with this grid-based method of energy evaluation provides a mechanism for the HIV-1P active site to be explored by the POM. A referee has noted that Autodock can be highly inaccurate for small molecules docked to large surfaces. Given that the POMs are large and rigid, we believe the problem to be minimal in this case. The results (see below) are certainly supportive. NPA charges and AutoDock van der Waals parameters were used for POM oxygens, since the terminal and bridging oxygens of the POM interact with the enzyme. Because tungsten and niobium Leonard-Jones parameters are not available in AutoDock, some van der Waals parameters are needed to account for the W and Nb atoms so that the POM does not end up in an unrealistic part of the grid. In other words, side chains of the enzyme can potentially experience favorable electrostatic interactions with the positively charged metals. If there is no van der Waals repulsion term to prevent this, parts of the enzyme could protrude into the center of the POM cage. Therefore, effective "dummy" atoms were used for W and Nb. In this case, carbon was substituted for tungsten and nitrogen for niobium. This is reasonable since all of these atoms are within the cage of the POM and do not directly interact with the enzyme. Carbon and nitrogen van der Waals parameters were selected because they both accomplish the prevention of enzyme penetration into the POM and permit an easy switch of carbon and nitrogen back to tungsten and niobium, respectively, at the end of the search.

Two AutoDock searches were undertaken. The first involved a search of the active site only. Two protonation states of HIV-1P were examined. In the first case only one of the Asp 25 carboxylates was protonated. In the second, both carboxylates were protonated. The overall charge on each HIV-1P is then +9 and +10, respectively. For each case, an 18 Å cubic grid ($90 \times 90 \times 90$ points with 0.2 Å spacings) centered at the active site was calculated. Each search entailed 100 runs, with 10 000 steps accepted or rejected before the termination of each run. Once a set was completed, the POM structures were converted to SYBYL mol2 format (with the appropriate charges and constraints added) and entered into a molecular database. Each of the resulting POM structures was then merged with HIV-1P and 100 steps of steepest descent minimization were carried out with a 16 Å nonbonded cutoff and a dielectric constant of 4.0. The structures with the lowest energies were examined in further detail.

The second search allowed the POM to explore the entire surface of the enzyme. Only the singly protonated (Asp 25) HIV-1P case was examined. A larger 63 Å cubic grid ($127 \times 127 \times 127$ points with 0.5 Å spacings) centered on the enzyme was computed. Because the outer surface of the enzyme is exposed in effect to a vacuum, a dielectric constant of 4.0 was employed when calculating the grid energies to dampen the electrostatics. The search entailed 100 runs, with 25 000 steps to be accepted or rejected before the end of each run to increase the likelihood that the POM would be able to explore most of the grid. The POM started each run at the center of the grid.

Results and Discussion

Synthesis. The α_1- and α_2-monoperoxyniobium-substituted Wells−Dawson complexes, α_1**1** and α_2**1**, respectively, were prepared by addition of the appropriate defect or lacunary POM to an aqueous H_2O_2 solution of hexaniobate. The corresponding monooxoniobium complexes, α_1**2** and α_2**2**, were prepared by refluxing the reaction mixture for 72 to 96 h before isolation of the product. The α_1 precursor lacunary species, α_1-$[P_2W_{17}O_{61}]^{10-}$, converts slowly to the corresponding α_2 isomer under the reaction conditions. As a consequence, Li^+ ions were added to the preparation as these are known to slow the α_1-to-α_2 isomerization relative to the corresponding K^+ salts.[63] All additional details for workup, isolation, and purification of the four complexes are given in the Experimental Section. The spectroscopic (^{31}P NMR, ^{183}W NMR, IR) and analytical data confirm the identity and purity of the products. All products were of 99+% chemical purity and 95 to 99% isomeric (α_1 versus α_2) purity. The α_1 isomer (niobium substituted in the belt of the Wells−Dawson polyanion; see Figure 1A) has C_1 symmetry and exhibits two ^{31}P NMR resonances in a 1:1 ratio at −11.0 and −12.5 ppm for the peroxo complex and −10.7 and −12.5 ppm for the oxo complex. The ^{183}W NMR exhibits 17 comparably intense resonances in the chemical shift range from −123.4 to −213.3 ppm for the peroxo complex and −121.3 to −208.1 ppm for the oxo complex. The $^2J_{wow}$ coupling could be observed for α_1**1** and varied from 17 to 28 Hz. This coupling could not be observed for α_1**2**. Low solubility of even

(90) Goodsell, D. S.; Olson, A. J. *Proteins: Struct., Funct., Genet.* **1990**, *8*, 195−202.

Table 3. HIV-1P Inhibition, Antiviral Activity, and Cytotoxicity Exhibited by Polyoxometalates

polyoxometalate	MW (g/mol)	IC_{50} (HIV−1P) (μM)[a]	anti-HIV-1 activity in PBMC, EC_{50} (μM)[b]	cytotoxicity in PBMC, IC_{50} (μM)[b]
$(NH_4)_{14}[NaP_5W_{30}O_{110}]$	7706	5.5	0.32	ND[c]
$(TMA)K_2[W_5NbO_{19}]$[d]	1468	NA[e]	>100	>100
α-$(NH_4)_6[P_2W_{18}O_{62}]$	4471	1.5	0.91	3.8
$K_{10}[\alpha_2$-$P_2W_{17}O_{61}]$	4554	86	0.14	66
$K_7[\alpha_1$-$P_2W_{17}(NbO_2)O_{61}]$ (α_1**1**)	4562	2.0	0.78	46
$K_7[\alpha_2$-$P_2W_{17}(NbO_2)O_{61}]$ (α_2**1**)	4562	1.2	0.81	74
$K_7[\alpha_1$-$P_2W_{17}NbO_{62}]$ (α_1**2**)	4546	1.5	0.83	>100
$K_7[\alpha_2$-$P_2W_{17}NbO_{62}]$ (α_2**2**)	4546	1.8	0.17	50

[a] None of the compounds inhibited pepsin at 100 μM. [b] PBMC = peripheral blood mononuclear cells. [c] Not determined. [d] TMA = tetramethylammonium. [e] Too low to be measured at solubility limit.

the lithium-exchanged salt of α_1**2** precluded acquisition of sufficient signal-to-noise to observe this coupling. The α_2-isomers (niobium substituted in the cap of the Wells−Dawson polyanion; see Figure 1B) of C_s symmetry exhibit two ^{31}P NMR resonances in a 1:1 ratio at −10.9 and −12.8 ppm for the peroxo complex and −10.7 and −12.9 ppm for the oxo complex and nine ^{183}W NMR resonances in a 2:2:1:2:2:2:2:2:2 ratio in a chemical shift range from −107.7 to −189.5 ppm for the peroxo complex and a similar nine-line spectrum from −109.5 to −198.2 ppm for the oxo complex. The $^2J_{wow}$ coupling was observed for both these complexes and ranged from 19 to 24 Hz for α_2**1** and from 14 to 24 Hz for α_2**2**.

The infrared spectra of the complexes are similar to that of the parent Wells−Dawson complex, $[P_2W_{18}O_{62}]^{6-}$. The O−O stretching fundamental is not visible, however, as this absorbance lies under the broad W−O stretching manifold. The presence of a peroxo group in α_1**1** and α_2**1** was confirmed, however, by the orange (α_1**1**) or yellow (α_2**1**) color of the complexes and quantified by iodometric titration.

pH Stability. The following information was obtained from the pH stability evaluations: (1) α_2**2** forms dimers in acidic aqueous solutions, while α_1**2** does not based on the well-documented and prominent asymmetric stretch of the linear Nb−O−Nb unit in the midinfrared (682 cm^{-1}).[91−94] Dimerization of oxoniobium(V) centers in POMs is a well-documented process, but steric differentiation between two nearly equivalent sites in a POM based on this condensation reaction is not. Indeed, the steric differences at surface sites in the Wells−Dawson structure (belt or α_1 versus cap or α_2), as those in the Baker−Figgis isomers of the parent Keggin structure (α, β, γ, δ, and ϵ),[95] are minimal and not differentiated by chemical reactivity. Thus the present case is noteworthy. The selective dimerization through the cap site (α_2) in these Wells−Dawson POMs is consistent with the slightly more crowded environment around the belt site (α_1) than the cap site in this common structure. The greater steric hindrance around the belt sites is apparent from examination of the X-ray structures of $[Nb_3P_2W_{15}O_{62}]^{9-}$ [76] and $[(NbO_2)_6P_2W_{12}O_{56}]^{12-}$.[92] The acid-induced dimerization reaction adds a dynamic aspect to this steric difference. (2) α_1**2** breaks down into free phosphate above pH 7. (At a pH of 6.8 no free phosphate was detected for α_2**2**.) (3) Even at a pH of 8, no evidence was found for the formation of free phosphate for α_2**1**. (4) All four of the title complexes appear to be stable up to a pH of 7.0.

Biological Data. Table 3 gives the inhibitory concentrations (IC_{50} values) for inhibition of purified HIV-1P by the two monoperoxoniobium POMs, α_1**1** and α_2**1**, the two monooxoniobium compounds, α_1**2** and α_2**2**, and other selected POMs. In addition it also gives two cell culture indicators: the anti-HIV-1 activity (effective concentrations for 50% suppression or EC_{50} values) and the cytotoxicity for 50% inhibition (inhibitory concentrations or IC_{50} values) for all these POMs. α_1**1**, α_2**1**, α_1**2**, and α_2**2** are all active against HIV-1P (IC_{50} values between 1 and 2 μM), highly active in cell culture against HIV, and noncytotoxic. The other POMs in Table 3 were prepared, purified, and evaluated under identical conditions. First, the parent literature Wells−Dawson polytungstodiphosphate, α-$[P_2W_{18}O_{62}]^{6-}$, was examined. The caveat on this compound, unlike that on α_1**1**, α_2**1**, α_1**2** and α_2**2**, is that it is thermodynamically unstable to hydrolytic fragmentation above pH 4.5.[63] The biological evaluations were conducted at pH 5.0. While α-$[P_2W_{18}O_{62}]^{6-}$ is highly active (IC_{50} = 1.5 μM), this number is not significant as it reflects the activities of $[P_2W_{18}O_{62}]^{6-}$ itself and a distribution of daughter POMs derived from this complex that are present over the duration of the evaluation. In contrast, the Pope−Jeannin−Preyssler ion, $[NaP_5W_{30}O_{110}]^{14-}$, and the monosubstituted Lindqvist ion, $[W_5NbO_{19}]^{3-}$, are both hydrolytically stable at the pH of biological evaluations.[51,64] $[NaP_5W_{30}O_{110}]^{14-}$ and $[W_5NbO_{19}]^{3-}$ were chosen as examples of globular POMs with substantially larger and smaller radii, respectively, than the title complexes, α_1**1**, α_2**1**, α_1**2**, and α_2**2**. While $[NaP_5W_{30}O_{110}]^{14-}$ is quite active (IC_{50} = 5.5 μM), $[W_5NbO_{19}]^{3-}$ is almost inactive (the activity is too low to be measured at the solubility limit of the complex, ~5 μM). As in the case with the activity of POMs against HIV-1 in cells,[25,43,49] there may be a threshold size below which POMs do not exhibit significant activity against HIV-1P.

Molecular Modeling. An outline of the computational approaches, the sources of data including the enzyme and POM structures, and the potential advantages and limitations of the methods used (and our efforts to address them) are elaborated in the Experimental Section. The results of the computational strategies are presented and discussed here. We address this research before the POM-HIV-1P inhibition kinetics and binding as the latter were conducted after the modeling and were intellectually defined by and constructed from the modeling results. As the POM-HIV-1P inhibition kinetics and binding data below agree to a remarkable degree with the predictions of the following modeling work, they impart additional validity to the modeling protocols and conclusions.

Sterics. HIV-1P is a homodimer held together via a salt bridge between the guanidinium group of Arg8 and Arg108 and Asp29 and Asp129.[8,11] A detailed summary of the HIV-1P active

(91) Finke, R. G.; Droege, M. W. *J. Am. Chem. Soc.* **1984**, *106*, 7274−7277.
(92) Judd, D. A.; Chen, Q.; Campana, C. F.; Hill, C. L. *J. Am. Chem. Soc.* **1997**, *119*, 5461−5462.
(93) Harrup, M. K.; Kim, G. S.; Zeng, H.; Johnson, R. P.; VanDerveer, D.; Hill, C. L. *Inorg. Chem.*, **1998**, *37*, 5550−5556.
(94) Kim, G.-S.; Zeng, H.; VanDerveer, D.; Hill, C. L. *Angew. Chem., Int. Ed. Engl.* **1999**, *38*, 3205−3207.
(95) Pope, M. T. *Heteropoly and Isopoly Oxometalates*; Springer-Verlag: Berlin, 1983.

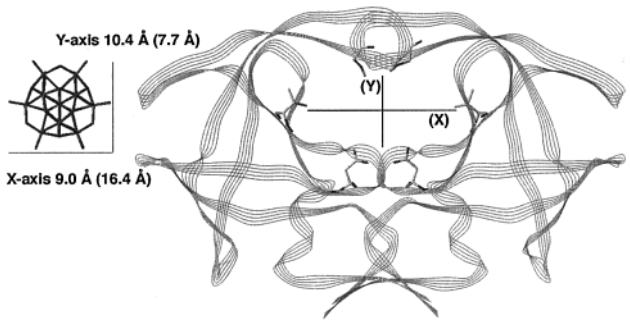

Figure 2. Measurements of the height and width (*x*- and *y*-axes) of the POM and the closed form of the HIV-1P active site. The POM values are before the parentheses and the HIV-1P active site values are inside the parentheses. The excessive bulk of the POM in the *y*-axis dimension precludes binding.

site structural features has been given by Meek.[13] The active site contains two catalytic triads, one in each subunit consisting of an aspartic acid, a threonine, and a glycine residue. The active site is highly conserved among all four enzyme/inhibitor complexes examined in this study, and its geometry is consistent with the diol transition state interaction model. The latter postulates the formation of a diol intermediate during hydrolysis of a peptide.[13] Figure 2 illustrates the closed form active site region and the end view of the Wells−Dawson POM structure, specifically α_2-$[P_2W_{17}NbO_{62}]^{7-}$ (α_2**2**). The end view shows the shorter *x* and *y* dimensions of the complex (9.0 and 10.4 Å, respectively). The enzyme and the POM are on the same size scale with key distances given in angstroms. The crucial distances used to define the active site are between hydrophobic residues, Val32 and Val32′, in the S1 and S1′ binding pockets for the width (*x* axis), and between catalytic aspartyl groups (D25 and D25′) and isoleucine residues (I50 and I50′) for the height (*y* axis). These distances are illustrated in Figure 2 as 16.4 and 7.7 Å, respectively, and were found to vary by no more than 1.2 Å in each direction among all four inhibitor-bound HIV-1P structures examined. The *z* dimension is defined by an axis passing through the center of the hole formed by the flaps closing over the active site.

Although the cylindrical shape of the anion appears to match the shape of the protease active site, the *y* dimension of the active site (7.7 Å) clearly cannot accommodate the 9.0 Å dimension of the POM. The transition state mimic inhibitors such as XK263, the DuPont-Merck cyclic urea, function by bridging the distance between the "flaps" at the top and the bottom of the active site groove. Although it is theorized that the "flaps" region may move inward as much as 7 Å during inhibitor binding,[13] the final bound structure in all enzyme/inhibitor complexes solved to date has the dimensions illustrated in Figure 2.

It is clear that the size of the POM will not allow it to bind analogous to known inhibitors. Given the activity for the virtually isostructural POMs α_1**1**, α_2**1**, α_1**2**, and α_2**2** in this study, we have the opportunity to investigate effective inhibitors of HIV-1P which may exhibit a completely new mechanism of action. Two possibilities for novel POM/HIV-1P binding are presented: (1) POM binding in the active site of the open form of HIV-1P or (2) POM binding on the external surface of HIV-1P (specifically the "hinge" regions).

Electrostatic Potential Surfaces. Manual docking of the POM Connolly surface within the Connolly surface of the HIV-1P active site indicates that the POM could sterically fit within the open form active site. However, the electrostatic potential surface mapped at the active site shows unfavorable negative charge. This is due in part to the presence of the catalytic aspartyl residues in their nonprotonated state. This negative charge would be reduced upon the expected protonation of one or both of the aspartates upon complexation. Further analysis of the HIV-1P surface reveals patches of positive charge near the "hinge" region of the flaps. This patch is a presentation of the underlying positive side chains (lysines 41, 43, 45,and 55). Upon closer inspection, surface and shape complimentarity is apparent as well. Each of these scenarios, POM docking in the open form of the active site and on the HIV-1P surface near the hinge regions, is now addressed.

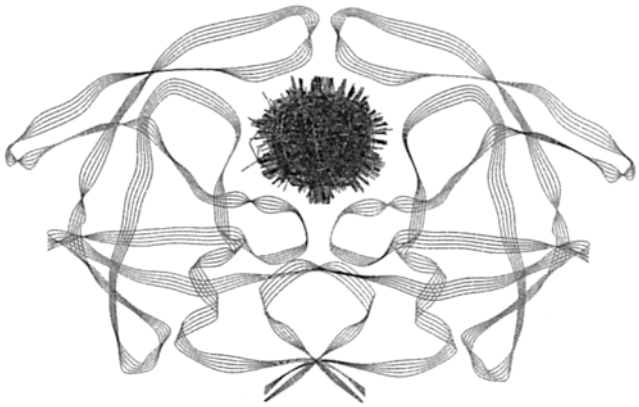

Figure 3. Positional conformers of the POM resulting from 100 AutoDock runs (search grid containing only the active site) superimposed within the open form of the HIV-1P active site.

Docking POM in Active Site. The POM active-site-only docking study for both protonation states of HIV-1P resulted in a family of 100 low-energy structures with the POM located in various binding positions as shown in Figure 3.

After optimization, the enzyme moved very little from its starting position, reflected by an RMS deviation less of than 0.1 A. Although the overall energy for the POM docking is lowered, consistent with expectation, it was decided to de-emphasize the energetic results. The level of approximation used in this modeling does not lend itself to accurate calculations of association energy. The energetics were used solely to select the conformer sets to be evaluated for structural explanations of binding. Compared to inhibitors crystallized within the active site of HIV-1P, the lowest energy structures for the POM docked in both the singly and doubly protonated (Asp 25 and Asp25/Asp125, respectively) enzymes exhibit high conservation of site interaction. It is important to note that the POM presents a similar electronic interaction environment for both a 120° rotation of the POM around its *z*-axis and a 180° rotation around the C_2 *y*-axis of the enzyme. This effect is seen in the family of structures with the lowest energies within the result set.

Key interactions between HIV-1P and the POM within hydrogen bonding distance include a terminal oxygen positioned between the Ile50 and Ile50′ residues of the enzyme flap, a central bridging oxygen in close proximity to protonated catalytic aspartyl residues, and a bridging oxygen in the niobium cap located near residues Arg 8 or Arg 8′. Interestingly, hydrogen bonding of the POM to the backbone atoms of the Ile50 residues is analogous to the hydrogen bonding of the conserved "301" water observed in the crystal structures of bound peptidomimetic inhibitors. Similarly, POM hydrogen bonds to the aspartyl residues have their counterparts in the H-bonding pattern seen in peptidomimetic inhibitors. The doubly protonated enzyme forms four hydrogen bonds to the POM. Finally, the H-bonding pattern of the Arg 8 residues is consistent with the same patterns observed in the only POM crystal

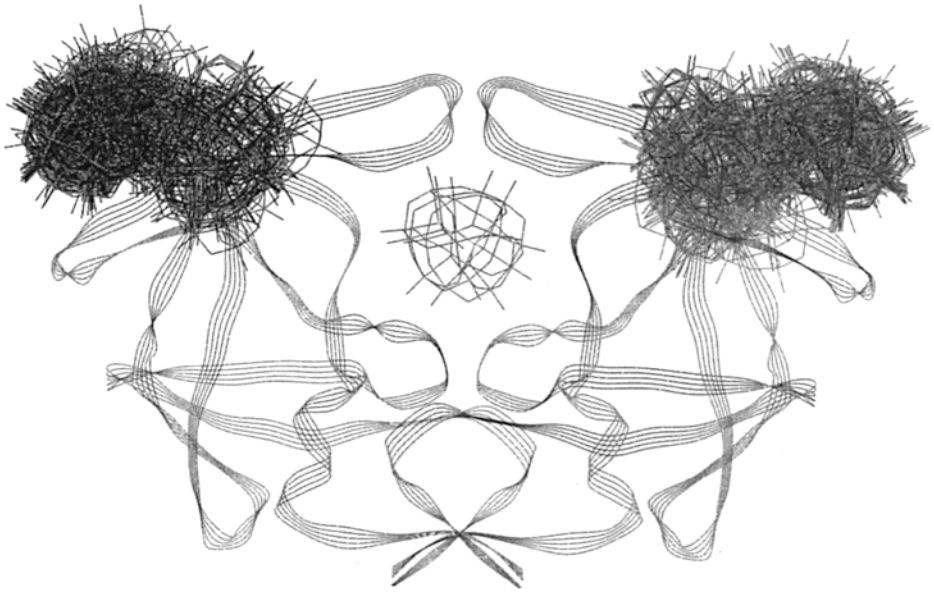

Figure 4. The results of an AutoDock study using a grid encompassing the entire HIV-1P surface. Out of 100 runs, 99 positional POM isomers migrated to the flap "hinge" regions, while one located itself at the active site.

structure where amino acid species are also present in the unit cell. In the latter study of Crans, Anderson, and co-workers, NH_4VO_3 was crystallized in the presence of the dipeptide salt Gly-Gly·HCl to form crystals of $[V_{10}O_{28}]^{6-}$ with interstitial glycyl-glycine units.[96] Both the ammonium and carboxylate terminii of the glycyl-glycine moieties are H-bonding to the oxygens of the POM.

POM Docking with the Entire Enzyme Surface. While molecular modeling predicts that POM binding to the active site of HIV-1P with the flaps open is possible, it predicts that a second mode of binding is more favorable still. This latter novel mode involves the anionic POM electrostatically binding to the previously mentioned cationic patch of lysine residues (lysines 41, 43, 45, and 55) on the hinge region of the flaps. The positive protein patch was apparent from the earlier qualitative inspection of the electrostatic potential mapped onto the Connolly surface of HIV-1P. Of the 100 AutoDock runs with the grid which encompasses the entire enzyme, 99 indeed show the POM interacting with the hinge regions of the protease, while one is located in the active site (Figure 4). Figure 5 illustrates the lowest energy POM-HIV-1P complex from the AutoDock study and highlights the salt-bridge interactions between POM oxygens and lysine terminal RNH_3^+ groups.

For the dimer to close when a substrate is in the active site, the aforementioned lysines must be displaced by 3−5 Å. Thus, if the negatively charged POM does interact noncovalently with these positively charged side chains, flap movement may be hindered or prevented. Hence, the dimer may not be able to close upon its substrate. This result illustrates a viable alternative explanation for POM inhibitory activity, one that we have shown to operate experimentally.

Comparison with Fullerenes and Haloperidol. Previously, two other systems have been proposed to bind to the open form of HIV protease with unusual binding modes, C_{60} (fullerene) derivatives, and haloperidol analogues. In the latter studies, the original 3-D database mining exercise identified bromperidol as an HIV protease inhibitor lead. The finding was accompanied by a $K_i = 100$ μM for the antipsychotic chloro analogue,

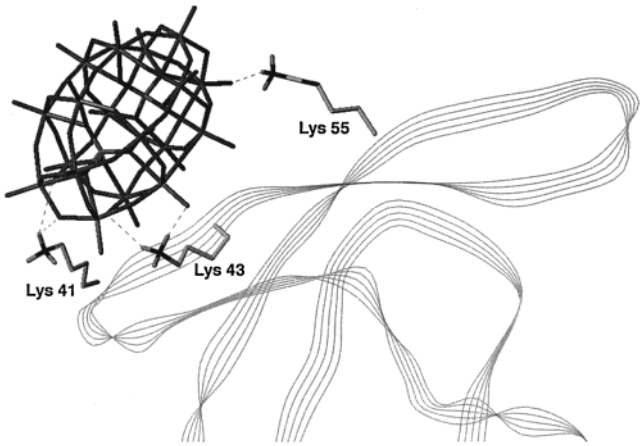

Figure 5. The lowest energy (KAA force field) POM structure from the AutoDock study involving an exploration of the entire HIV-1P enzyme (surface and active site). The POM terminal and bridging oxygens form hydrogen bonds to the lysine side chains of the HIV-1P "hinge region".

haloperidol.[97] Subsequent analogue development[98,99] and renewed database searching[100] has yielded compounds with K_i's ranging from 5 to 400 μM, a number of which operate by alkylating nonactive site thiol groups.[99] Accompanying X-ray crystallographic analyses have illustrated binding orientations at odds with both the predicted[99] and the peptidic[97,98,100] binding modes.

In the fullerene series, modeling studies suggested that the open form of the HIV-1P active site is sterically complementary to the shape of the hydrophobic fullerenes. As a result, the latter

(96) Crans, D. C.; Mahrooftahir, M.; Anderson, O. P.; Miller, M. M. *Inorg. Chem.* **1994**, *33*, 5586−5590.

(97) DesJarlais, R. L.; Seibel, G. L.; Kuntz, I. D.; Furth, P. S.; Alvarez, J. C.; Ortiz de Montellano, P. R.; DeCamp, D. L.; Babé, L. M.; Craik, C. S. *Proc. Natl. Acad. Sci. U.S.A.* **1990**, *87*, 6644−6648.

(98) Rutenber, E.; Fauman, E. B.; Keenan, R. J.; Fong, S.; Furth, P. S.; Ortiz de Montellano, P. R.; Meng, E.; Kuntz, I. D.; DeCamp, D. L.; Salto, R.; Rosé, J. R.; Craik, C. S.; Stroud, R. M. *J. Biol. Chem.* **1993**, *268*, 15343−15345.

(99) De Voss, J. J.; Sui, Z.; DeCamp, D. L.; Salto, R.; Babé, L. M.; Craik, C. S.; Ortiz de Montellano, P. R. *J. Med. Chem.* **1994**, *37*, 665−673.

(100) Rutenber, E.; De Voss, J. J.; Hoffman, L.; Stroud, R. M.; Lee, K. H.; Alvarez, J.; McPhee, F.; Craik, C. S.; Ortiz de Montellano, P. R. *Bioorg. Med. Chem.* **1997**, *5*, 1311−1320.

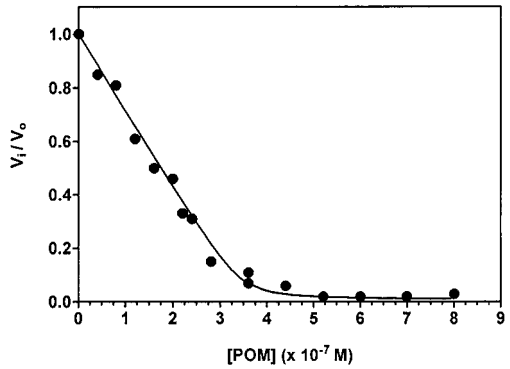

Figure 6. Residual HIV-1P activity at different concentrations of POM (α_2**2**). V_o and v_i are initial activities in the absence and presence of POM. These data were used in K_i determinations. The above experimental data were determined with 0.15 μM HIV-1P and 0.15 mM chromogenic substrate in an acetate buffer with 0.1 M NaCl (see Experimental Section).

compounds were proposed as HIV-1P inhibitors, and a derivative with a competitive binding constant of 5 μM was prepared.[23] No X-ray crystallographic investigations have yet provided structural verification of the proposed complexes, nor have the compounds been reported to rescue HIV-infected cells. However, a very recent study modeled candidate inhibitors into the open HIV-1P binding site and based synthetic priority on the extent of hydrophobic surface area desolvation.[101] Two compounds were prepared which show HIV-1P binding affinities from 100 to 150 nM at high salt concentration. In view of the similar steric requirements of the POMs (Figure 3), had we adopted arguments similar to those used for inhibition by the fullerene derivatives, our predictions would have been inconsistent with the subsequent binding studies.

The POMs are superior to the unconventional compound classes mentioned above in that they exhibit greater potency as antivirals against HIV and as inhibitors of HIV-1P to the extent of 1 and 3 orders of magnitude, respectively. Furthermore, ambiguity concerning the details of binding mode as it relates to classical HIV-1P inhibitors is not an issue. We predict and the kinetic studies clearly show that noncovalent binding is distinct from the protein's active site. Precise geometrical parameters will be defined only when an X-ray crystal structure has been determined.[102]

Stoichiometry and Inhibition Constant for POM ($\alpha_2$2) with HIV-1P. Both of these parameters were readily derived by standard methods described in the Experimental Section. Figure 6 gives representative data in the form of a plot of residual HIV-1P activity at varying concentrations of α_2**2**. The K_i values are 1.1 $\pm$ 0.5 and 4.1 $\pm$ 1.8 nM in 0.1 and 1.0 M NaCl, respectively. The data also permitted calculation of the enzyme (HIV-1P homodimer) to inhibitor (α_2**2**) association stoichiometry. It is 1:2 in both cases, in excellent agreement with the results of the previously conducted modeling investigations.

Inhibition Kinetics of HIV-1P by the POM ($\alpha_2$2). To establish the mechanism of inhibition of HIV-1P by α_2**2**, the steady-state kinetics of this inhibition were studied. Figure 7 shows plots of the reciprocal initial velocity versus the reciprocal substrate concentration in the absence and presence of α_2**2** at three concentrations. It is clear that the k_{cat} but not K_m values

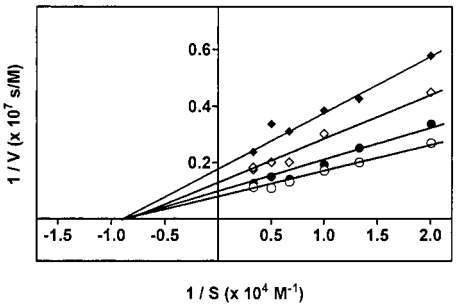

Figure 7. Lineweaver−Burk plot of HIV-1P activity in the presence and absence of POM (α_2**2**). The reciprocal initial velocity values are plotted against reciprocal substrate concentrations. The K_m values of 0.13, 0.12, 0.13, and 0.13 mM and k_{cat} values of 8.1, 7.7, 5.3, and 3.9 s^{-1} were determined with 0 (○), 40 (●), 100 (◇), and 140 (◆) nM POM, respectively.

are affected by the presence of the POM. These steady-state kinetics results establish that POM inhibition of HIV-1P is the noncompetitive type which effectively rules out POM binding to the active-site cleft of HIV-1P. This is not surprising given the marked differences in physical and electronic structure of the POMs versus the natural polypeptide HIV-1P substrates. The noncompetitive inhibition is in full agreement, however, with the clear inferences from both the modeling and binding results, namely that the POM is binding strongly to a site remote from the active site.

Conclusions

(1) Four polyoxometalates (POMs) targeted to be stable at physiological pH (~7) have been prepared and characterized. All are of the Wells−Dawson POM structural class and contain either one peroxoniobium(V) or oxoniobium(V) unit substituted for one oxotungsten(VI) unit in the parent POM. The two isomeric peroxo complexes, α_1-$K_7[P_2W_{17}(NbO_2)O_{61}]$ (α_1**1**) and α_2-$K_7[P_2W_{17}(NbO_2)O_{61}]$ (α_2**1**), are prepared by treating the monodefect or lacunary forms of the POM, $[P_2W_{17}O_{61}]^{10-}$ with $[Nb_6O_{19}]^{8-}$, in aqueous H_2O_2. The corresponding oxo complexes, α_1-$K_7[P_2W_{17}NbO_{62}]$ (α_1**2**) and α_2-$K_7[P_2W_{17}NbO_{62}]$ (α_2**2**), are obtained by refluxing the peroxo analogues in H_2O. The spectroscopic (^{31}P NMR, ^{183}W NMR, IR) and analytical data confirm a 99+% chemical purity and 95 to 99% isomeric (belt or α_1 versus cap or α_2) purity of all four POMs.[50]

(2) Unlike the parent POM, $[P_2W_{18}O_{62}]^{6-}$, α_1**1**, α_2**1**, α_1**2**, and α_2**2** all appear to be stable up to pH 7.0.

(3) The greater steric congestion about the belt site (α_1) compared to the cap site (α_2) in the Wells−Dawson structure is indicated by a chemical reaction, the acid-induced dimerization of oxoNb(V) units through Nb. The cap-substituted complex, α_2**2**, dimerizes; the belt-substituted complex, α_1**2**, does not.

(4) All four complexes are highly active in cell culture against HIV-1 (EC_{50} values: 0.17−0.83 μM) and minimally toxic (IC_{50} values: 50 to >100 μM) (peripheral blood mononuclear cells for both assays). In addition, all four complexes exhibit significant activity against purified HIV-1 protease (HIV-1P) (IC_{50} values for α_1**1**, α_2**1**, α_1**2**, and α_2**2**: 2.0, 1.2, 1.5, and 1.8 μM, respectively) and had no effect at 100 μM against pepsin.

(5) A general protocol for examining POMs by using force fields or grid-based methods designed to carry out protein calculations has been developed. In this study, steric features of the POM and HIV-1P were measured within Sybyl 6.2. Molecular mechanics parameters were developed for the POM by fixing its bond lengths and angles and determining charges

(101) Friedman, S. H.; Ganapathi, P. S.; Rubin, Y.; Kenyon, G. L. *J. Med. Chem.* **1998**, *41*, 2424−2429.

(102) Attempts to crystallize HIV protease in the presence of various POMs have so far been unsuccessful. We appreciate the efforts of John Erickson, NCI, in this respect.

from NPA analysis at the HF/LANL2DZ level of theory. AutoDock was employed to allow the POM to explore the HIV-1P active site and external surface. Finally, the Kollman all-atom force field with the aforementioned POM parameters was used for structure optimization and qualitative energy assessments of the AutoDock results. Using a similar procedure to the one presented in this study, a POM from any structural class can be examined in the context of an enzyme.

(6) Molecular modeling strongly points to a mode of interaction between the representative POM $[P_2W_{17}NbO_{62}]^{7-}$ (α_2**2**) and HIV-1P that involves POM binding at the cationic pocket in the "hinge" region on the outside of the flaps covering the active site of the enzyme. It rules out POM binding in the conventional "flaps closed" form of the active site but not the "flaps open" form of the active site. The latter, however, is significantly less favorable than binding to the hinge region of the flaps. The modeling research clearly defined POM-HIV-1P binding and inhibition kinetics studies that would address this new mode of HIV-1P inhibition.

(7) Data on the residual HIV-1P activity as a function of POM (α_2**2**) concentration under varying conditions indicated a stoichiometry of association of 2 POMs per HIV-1P homodimer and a very strong inhibition constant ($K_i = 1.1 \pm 0.5$ and 4.1 ± 1.8 nM in 0.1 and 1.0 M NaCl, respectively). In addition, extensive steady state inhibiton kinetics of HIV-1P by this POM clearly indicated the inhibiton was noncompetitive.

(8) All the modeling and experimental data are mutually consistent and collectively make a strong case for a heretofore uncharacterized selective mode of HIV-1P inhibition−inhibitor binding remote from the enzyme-active site in a cationic pocket of lysine residues on the outer surface of the flaps that cover the active site. Enzymatic and crystallographic studies using wild-type and mutant HIV-1P are planned to further substantiate these conclusions.

Acknowledgment. C.L.H. and R.F.S. thank the National Institutes of Health (grant no. AI-32903), J.T. thanks the NIH (grant AI 38189), C.L.H. thanks the Office of Naval Research (Molecular Design Institute; grant N00014-95-1-1116), and R.F.S. thanks the Department of Veterans Affairs and the Georgia VA Research Center for AIDS and HIV Infections for support. We thank Helga Cohen of the NMR Center at the University of South Carolina for obtaining some of the ^{183}W NMR spectra, Lin Hong for collection of some of the data in Table 3, Jeff Rhule for assistance in manuscript preparation, and Angie McMillan for technical assistance.

JA001809E